Errors Resulting From the Reflectivity of Calibration Targets

James Randa, *Senior Member, IEEE*, David K. Walker, *Member, IEEE*, Amanda E. Cox, *Member, IEEE*, and Robert L. Billinger

***Abstract*—For a microwave total-power radiometer, we consider the error introduced by neglecting the difference in the antenna reflection coefficient between when it views a distant scene and when it views a nearby calibration target. An approximate expression is presented for the error, and measurements are described that enable one to estimate the resulting uncertainty in the measured brightness temperature. The measurement results are presented for several combinations of antenna and calibration target. The resulting uncertainty ranges from about 0.1 K to several kelvins for the representative cases considered.**

***Index Terms*—Calibration, calibration target, microwave radiometry, radiometer, remote sensing, uncertainty analysis.**

I. Introduction

THE ABSOLUTE accuracy of microwave remote sensing radiometers is an important consideration for many applications. One method of achieving absolute radiometer calibration is through the use of blackbody calibration targets to provide reference brightness temperatures for the radiometer to view. These targets are widely used with spaceborne, airborne, and ground-based microwave instruments. While studies have been published that assess overall instrument calibration performance [1], [2] or calibration methods [3], [4], or identify error sources relative to specific instruments or groups of instruments [5], [6], few studies exist which investigate the calibration target-related sources in detail.

In the calibration of microwave remote sensing radiometers, it is not uncommon for calibration targets to be relatively close to the sensing antenna, whereas the calibrated radiometer is used to measure very distant objects. Such a situation can occur, for example, when using "close-coupled" calibration targets for a radiometer used in remote sensing of the earth's surface from an airplane or satellite. There are two general types of errors that this arrangement can introduce for a total-power radiometer. One is that antenna–target interactions can affect the properties of the antenna such as its pattern and directivity, which may, therefore, be different when calibrating the radiometer than when viewing the earth. A second type of error is introduced by the change of the reflection coefficient at the antenna output (i.e., at the reference plane between antenna and receiver) due to reflections from the calibration target that are not present when viewing a distant target. This difference in reflection coefficients results in different mismatch factors, and it also gives rise to changes in the system noise figure and available gain if the radiometer does not have an input isolator. The effects due to target proximity are distinct from errors arising from imperfections in the target itself—such as temperature gradients or uncertainty in the emissivity [6]–[8]. Target characterization and scattering from the target are of great concern, but they are not the subject of this paper. Here, we concern ourselves only with the target-proximity errors.

For an ideal blackbody calibration target, both the target-proximity effects vanish, and for a very good target they are "very small." With modern microwave radiometers striving for ever smaller uncertainties, however, it becomes important to determine these effects. An uncertainty of 0.1 K or better, which some radiometers hope to achieve, is about 0.03% of 290 K, and it is not immediately obvious that target-proximity effects are negligible at that level. In this paper, we consider the second type of error, that introduced by the difference in the antenna reflection coefficient when the antenna is pointed at a nearby calibration target as opposed to a very distant scene of interest. We first derive equations for the error introduced by ignoring this difference. We then describe measurements performed on several different antenna–target combinations, measuring the difference in reflection coefficient for near and far targets. The size of the effect also depends on the noise parameters of the radiometer, and we measured these for a particular instrument. This allows us to estimate the magnitude of the error incurred when the effect is neglected. In all the analysis, we assume a total-power radiometer.

The remainder of the paper is organized as follows. Section II derives the equations for the error. Section III describes the measurements and presents the results. Section IV contains the numerical estimates of the resulting errors and a discussion of their significance, and Section V is devoted to a discussion and summary of the work.

II. Calculation

We use uppercase P to denote available spectral power and lowercase p to denote delivered spectral power. At a given reference plane, such as 1, the two are related through the mismatch factor M, $p_1 = M_1 P_1$. For most purposes in this paper, the only reference plane of interest is that between the antenna and the rest of the radiometer, plane 1 in Fig. 1. When the antenna is

Manuscript received December 31, 2003; revised August 4, 2004.

J. Randa, D. K. Walker, and R. L. Billinger are with the Electromagnetics Division, National Institute of Standards and Technology, Boulder, CO 80305 USA (e-mail: randa@boulder.nist.gov).

A. E. Cox was with the National Center for Atmospheric Research and Department of Aerospace Engineering Sciences, University of Colorado, Boulder, CO 80307 USA and is now with the Electromagnetics Division, National Institute of Standards and Technology, Boulder, CO 80305 USA.

Digital Object Identifier 10.1109/TGRS.2004.839809

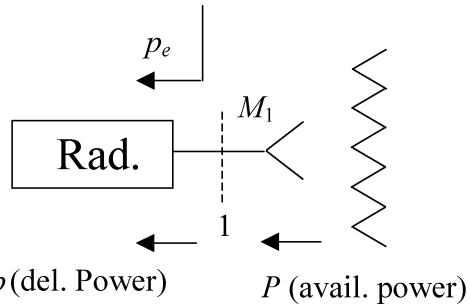

Fig. 1. Antenna viewing calibration target.

pointed at a calibration target, as in Fig. 1, the spectral power delivered to the radiometer at plane 1 can be written as

$$p_h = M_h P_h + p_{e,h} \tag{1}$$

where M_h is the mismatch factor at plane 1 when the antenna is viewing the hot calibration target, P_h is the available spectral power at plane 1 from that target, and $p_{e,h}$ is the effective delivered spectral power at the input plane 1 due to the radiometer's intrinsic noise (when the antenna is viewing the hot calibration target). The quantity $p_{e,h}$ is related to the effective input noise temperature T_e of the receiver by $p_{e,h} = kM_h T_{e,h}$, where k is the Boltzmann constant. The mismatch factor is the ratio of delivered power to available power at the given reference plane; in terms of the reflection coefficients at plane 1, it is given by

$$M_0 = \frac{\left(1 - |\Gamma_{\text{ant}}|^2\right)\left(1 - |\Gamma_r|^2\right)}{|1 - \Gamma_{\text{ant}}\Gamma_r|^2}$$

where Γ_{ant} is the reflection coefficient from the antenna (at plane 1), and Γ_r is the reflection coefficient from the radiometer receiver. P_h is related to the noise temperature at the output of the antenna by $P_h = kT_h$. Similar equations can be written for the delivered power when the antenna views the cold calibration target (c) and the unknown scene (x). The three equations can be combined and solved for T_x to obtain the radiometer equation. To simplify matters, we assume that the antenna's reflection coefficient is the same when it is viewing the cold calibration target as when it is viewing the hot target, so that $M_c = M_h$ and $p_{e,c} = p_{e,h}$. The radiometer equation then takes the form

$$T_x - T_c = \frac{M_h}{M_x}\left[\frac{(p_x - p_c) - (M_x - M_c)P_c - (p_{e,x} - p_{e,c})}{(p_h - p_c)}\right] \times (T_h - T_c). \tag{2}$$

If the reflection coefficient of the antenna at plane 1 is the same whether the antenna views the hot target, the cold target, or the unknown, then $M_x = M_c = M_h$, $p_{e,x} = p_{e,c}$, and (2) reduces to

$$T_x - T_c = \frac{(p_x - p_c)}{(p_h - p_c)}(T_h - T_c). \tag{3}$$

Equation (3) is the form of the (total-power) radiometer equation that is commonly used in remote sensing radiometry. In order to consider the errors introduced by using (3) when the antenna reflection coefficient is different for calibration targets and the distant scene, we can rewrite (2) in the form

$$T_x - T_c = (T_x - T_c)_0(1 + \delta_1) + \Delta_2 + \Delta_3 \tag{4}$$

where

$$\begin{aligned}(T_x - T_c)_0 &= \frac{(p_x - p_c)}{(p_h - p_c)}(T_h - T_c)\\ \delta_1 &= \frac{M_h}{M_x} - 1\\ \Delta_2 &= -\frac{M_h}{M_x}\frac{(M_x - M_h)P_c}{(p_h - p_c)}(T_h - T_c)\\ \Delta_3 &= -\frac{M_h}{M_x}\frac{(p_{e,x} - p_{e,c})}{(p_h - p_c)}(T_h - T_c).\end{aligned} \tag{5}$$

The $(T_x - T_c)_0$ term is the answer that one would obtain using (3). The δ_1 term is due to the different mismatch factors, and Δ_2 and Δ_3 result from the system's different available gain and noise temperature when the antenna reflection coefficient changes. As can be seen from (4), δ_1 is a fractional error in $(T_x - T_c)$, whereas Δ_2 and Δ_3 are additive errors.

Because our purpose is to estimate the magnitudes of the probable errors rather than to make exact corrections for them, we can make some simplifying assumptions. We have already assumed that the antenna's reflection coefficient is the same when it is viewing the cold calibration target as when it is viewing the hot target. We use Γ_c to denote the antenna reflection coefficient when it is viewing either calibration target, Γ_∞ for when the antenna is pointed at the distant scene, and Γ_r for the reflection coefficient of the radiometer at plane 1. We first assume that the effect is small, and so we keep only the lowest nonvanishing order in $\Delta\Gamma \equiv \Gamma_c - \Gamma_\infty$. We then also assume that each of the reflection coefficients Γ_c, Γ_∞, and Γ_r is small and save only terms to the lowest order in the reflection coefficients. With these approximations and some tedious algebra (sketched in Appendix A), the errors can be written as

$$\begin{aligned}\delta_1 &\approx 2\,\text{Re}\left[(\Gamma_r - \Gamma_\infty)\Delta\Gamma\right]\\ \Delta_2 &\approx 2T_c\,\text{Re}\left[(\Gamma_r - \Gamma_\infty)\Delta\Gamma\right] = \delta_1 T_c\\ \Delta_3 &\approx 2X_1\,\text{Re}(\Gamma_\infty\Delta\Gamma) + 2\,\text{Re}(X_{12}\Delta\Gamma)\end{aligned} \tag{6}$$

where X_1 and X_{12} are noise parameters of the radiometer [9]. They are elements of the noise correlation matrix in the wave representation, but referred to the input port. Thus, they are related to the noise correlation matrix of Wedge and Rutledge [10] by $kX_1 = \overline{|c_1|^2}$, $kX_{12} = \overline{c_1 c_2^*}/S_{21}^*$, where k is Boltzmann's constant, the c's are wave amplitudes of the radiometer's intrinsic noise, and S_{21}^* is the complex conjugate of the 21 element of the scattering matrix. Some additional detail is provided in Appendix A.

Equation (6) gives an approximation for the errors introduced by using the simplified radiometer equation, (3). To estimate those errors, we need to know or estimate Γ_r, Γ_∞, $\Delta\Gamma$, X_1, and X_{12}. Γ_r can be measured by a vector network analyzer. In the next section, we describe measurements of Γ_∞, $\Delta\Gamma$, and the noise parameters X_1 and X_{12}. We shall then return to obtaining actual numerical estimates of the errors in (6).

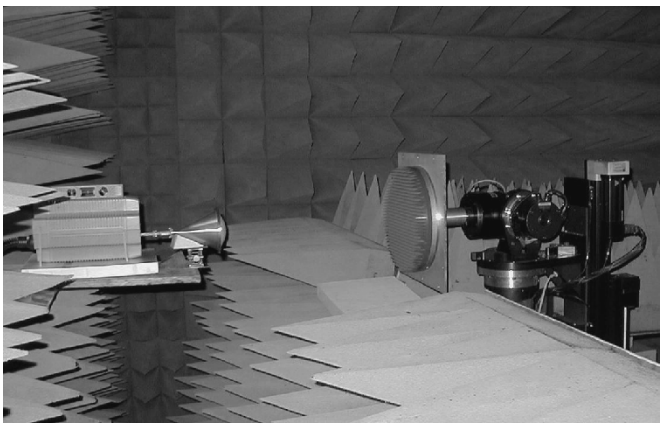

Fig. 2. Configuration for measurement of antenna reflection coefficient.

III. Measurements

A. Setup, Antennas, and Targets

Measurements were performed in the National Institute of Standards and Technology (NIST) anechoic chamber, whose dimensions between outer walls are $5\,\mathrm{m} \times 5\,\mathrm{m} \times 8\,\mathrm{m}$. A calibrated vector network analyzer was connected to the waveguide input of the antenna, and the antenna was mounted so that it pointed at the center of the target, which was mounted on a movable cart in the anechoic chamber. The absorber-covered cart runs on rails, and its position is computer controlled with a precision of 0.1 mm. The measurement setup is pictured in Fig. 2. The cart was stepped backward from the antenna, with the reflection coefficient of the antenna measured as a function of the distance from antenna to target. For each antenna, a measurement was also made with the target at the maximum distance allowed by the size of the anechoic chamber (about 4.5 m), to simulate viewing a distant scene. For practical reasons, the antennas and targets were not all measured with the same surrounding structure they would have in actual use. Although this could affect our quantitative results, we would expect the effect to be small, and it would not affect our general conclusions.

Several combinations of antenna and target were measured. All the targets were at room temperature (296 K) for the measurements. The first target, which will be referred to as the National Aeronautics and Space Administration (NASA) target, is a commercially produced circular disc approximately 33 cm in diameter, faced with an array of quadrahedral pyramids with an aspect ratio of $4:1$. The base material of the target is aluminum, with pyramids formed by electrical discharge machining and coated with ferrous-loaded epoxy with a thickness of about 1 mm. It is intended for use at frequencies above about 35 GHz. The antenna used with this target was a commercially produced WR-19 cylindrical horn antenna with a dielectric lens and approximately 12.7-cm aperture, intended for use from 51–56 GHz. At 53 GHz, its 3-dB beamwidth is 3° in the H plane and 2.8° in the E plane. It will be called the NOAA (National Oceanic and Atmospheric Administration) antenna. The combination of NOAA antenna and NASA target was measured from 50–57 GHz in 1-GHz increments, but we will present only the results for 54 GHz, near the middle of the antenna's intended range. The results at 54 GHz are representative of those at the other measurement frequencies; if anything, they may exhibit a smaller effect than at frequencies near the edge of the measurement range. The target was scanned over 10 mm, with measurements taken every 0.5 mm, starting from a minimum distance of about 2 cm between the antenna lens and the tips of the target. For comparison purposes, and because it is of interest to anechoic chamber users, measurements were also made on a target consisting of a piece of RF absorber like that used to line the anechoic chamber. It is carbon-impregnated foam with an array of 0.61-m-tall pyramids on 0.2-m centers. The target was a square with sides of length approximately 1.5 m. Two sets of measurements were made on the foam absorber, one with the tip of a pyramid aligned with the center of the antenna, and the other with the antenna pointed about half way between a tip and a valley. For the measurements on the foam absorber, a cart position of 0 corresponded to a distance of about 1 cm from the antenna aperture to the tips of the target pyramids.

Another set of measurements, using different antennas and targets, was performed at 0.5-GHz increments from 35–39 GHz. We will present only the results at 37 GHz, which is the nominal operating frequency of one of the antennas used. Results at other measurement frequencies are similar or show a larger effect. One target used in these measurements was the calibration target from the Airborne Imaging Microwave Radiometer (AIMR) [11]. This target is a commercially produced rectangular array of quadrahedral pyramids formed from a ferrous-loaded epoxy material molded on a bed of nails in an aluminum base. The array is covered with a polystyrene insulating layer and a mylar window roughly 0.25 mm thick. The overall transverse dimensions of the target are approximately 25×30 cm. The target was measured both with and without its cover; we will present the results with the cover in place since this corresponds to the configuration in which it is used. Two different antennas were used with the AIMR target. One was a standard-gain horn, and the other was a spare feed horn of the same design as the one used in AIMR. The standard-gain horn has a half-power beam width of 9.5° in the E-plane and 10.5° in the H-plane. Its aperture is 56.5 mm $\times$ 69 mm. The AIMR feed horn consists of a Gaussian optics lens antenna (GOLA), horn, dichroic plate, and grid polarizers. The half-power beam width at 37 GHz is 2.8°. The GOLA is mounted at the mouth of the feed horn and is constructed to reflect all energy below 30 GHz. The dichroic plate separates the beam into two frequencies, nominally 37 and 90 GHz, and the grid polarizers divide each frequency into orthogonal polarizations, to yield four independent channels. In the actual AIMR instrument, the antenna system consists of the feed horn and an elliptical scan mirror, but in the present measurements only the conical horn was used. As was done in the set of measurements at higher frequencies, measurements were also made with each of these antennas with a piece of carbon-loaded foam absorber as the target.

B. Measurement Results

Fig. 3 plots the magnitude of the reflection coefficient Γ_c of the NOAA antenna when it views the calibration target, as a function of the cart position, at 54 GHz. It also shows the result for very large distance (4.5 m), Γ_∞. Fig. 3 clearly shows the effect of the target on the reflection coefficient of the antenna. It

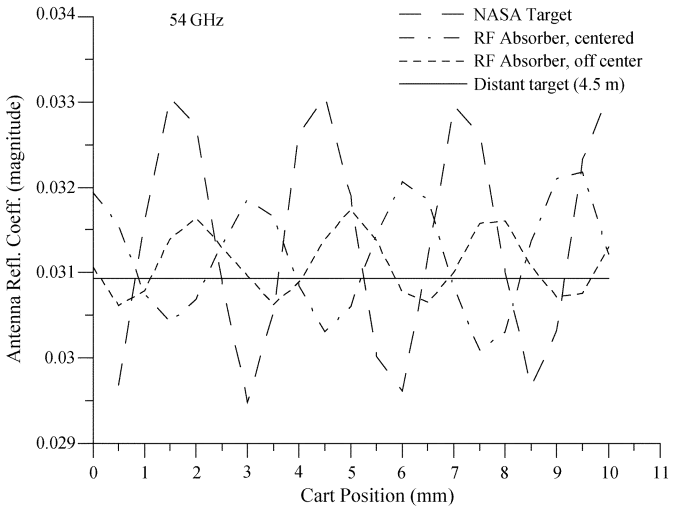

Fig. 3. Measured reflection coefficient of antenna as function of cart position.

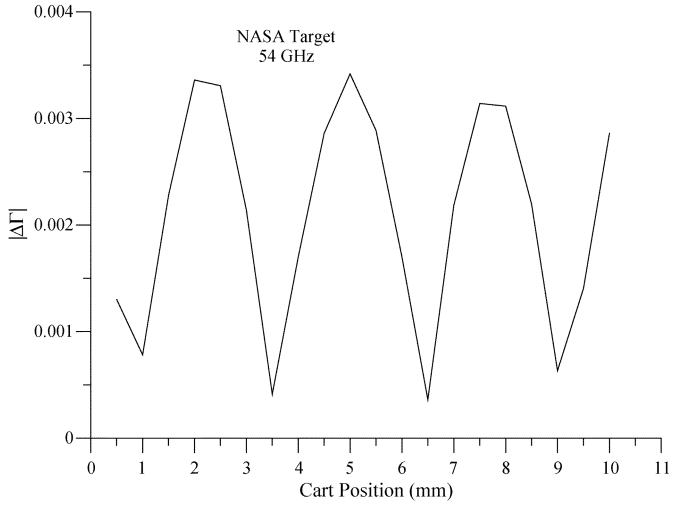

Fig. 4. Magnitude of $\Delta\Gamma$ for NASA target as function of cart position.

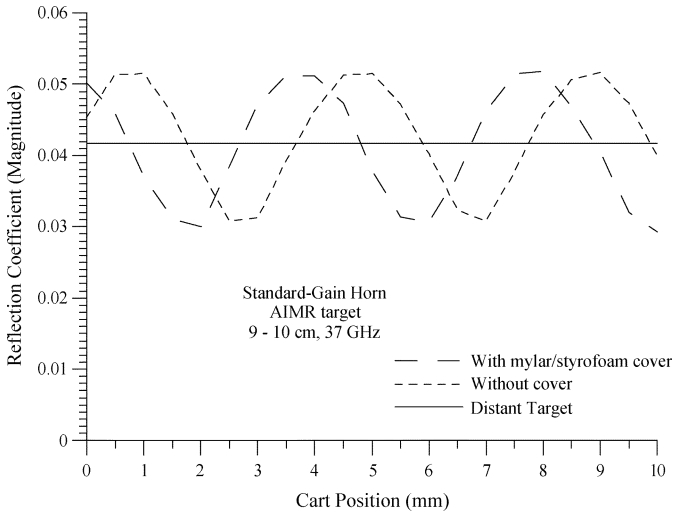

Fig. 5. Reflection coefficient of standard-gain horn viewing AIMR target, 9–10 cm.

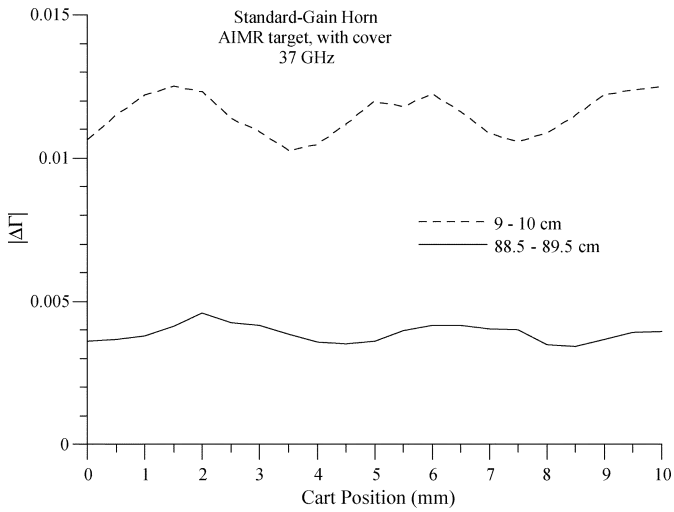

Fig. 6. $|\Delta\Gamma|$ for horn viewing AIMR target at 9–10 and at 88.5–89.5 cm.

is interesting to note that the effect is significantly (about two times) greater for the calibration target than for the foam absorber. Since the quantity of interest is actually $\Delta\Gamma = \Gamma_c - \Gamma_\infty$, we plot its magnitude in Fig. 4. We see that the magnitude of $\Delta\Gamma$ ranges from about 0.0005 to about 0.0035. The consequences of this will be considered in Section IV below.

The combination of a standard-gain horn with the AIMR target (both with and without the target cover) was measured over two ranges of distance (from antenna aperture to tips of target pyramids), from 9–10 and 88.5–89.5 cm. The 9–10-cm scan corresponded to the closest distance possible for the experimental setup. The 88.5–89.5-cm distance was chosen to correspond to the distance between the antenna aperture and the target in the actual AIMR instrument. The relevant distance was taken to be from the approximate phase center of the AIMR antenna (rather than from the aperture) to the tips of the target pyramids. Results for the magnitude of the reflection coefficient for the 9–10-cm scan are shown in Fig. 5. The flat, solid line is the result for a distant target. For the 88.5- to 89.5-cm scan, the results for the magnitude of the reflection coefficient are qualitatively similar, with the distant-target result again at about 0.042. Fig. 6 plots the magnitude of the difference between the reflection coefficient for a given target distance and the result for a distant target, $\Delta\Gamma = \Gamma_c - \Gamma_\infty$, which is needed in computing the error resulting from target reflectivity effects. The magnitude of $\Delta\Gamma$ is significantly larger for the scan at smaller distance, as would be expected. Because of the large distance, large beamwidth, and relatively small target, the 88.5–89.5-cm scan for the standard-gain horn and AIMR target represents by far the worst case of our measurement configurations for spillover of the beam from the target. For the 89.5-cm position, the spot size on the target, computed from the 3-dB beamwidth, is 14.8 cm $\times$ 16.4 cm, and the target size is 25 cm $\times$ 30 cm. Three other measurements were made with the standard-gain horn: a scan from 76 to 77 cm of a piece of the foam absorber that is used to line the anechoic chamber, and measurements of a flat metal plate (the cover of the NASA target) from 10–11 and 116–117 cm. The results for the foam absorber are shown in Fig. 7. The results from the flat metal plate show much larger antenna reflection coefficient and variation with distance, as expected, but we do not show them here.

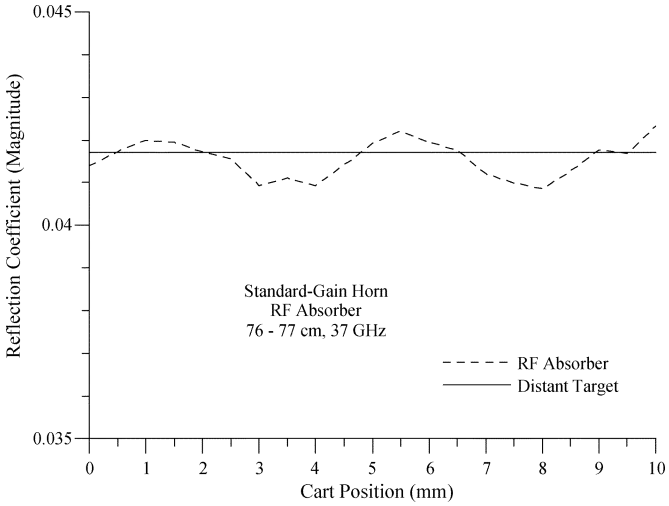

Fig. 7. Standard-gain horn viewing foam absorber.

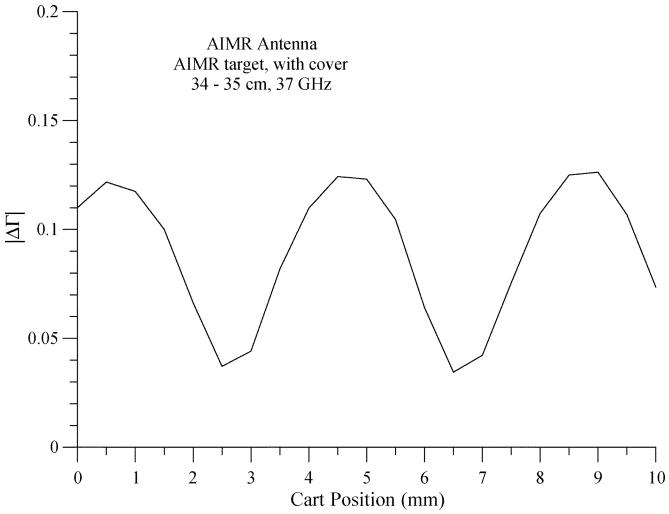

Fig. 8. $|\Delta\Gamma|$ for AIMR antenna and AIMR target.

Results for the reflection coefficient of the AIMR antenna viewing the AIMR target (with and without cover) for a scan from 34–35 cm look much like Fig. 5 and are not shown. The result for the distant target in this case is approximately 0.075. The 34–35-cm distance was chosen because it is the approximate distance between the AIMR antenna aperture and the target in the actual radiometer. The plot of $|\Delta\Gamma|$ for this scan is given in Fig. 8. Fig. 9 shows the results for measurements with the AIMR antenna and the RF absorber.

Several general qualitative features are apparent in the graphs. The reflection coefficient of the AIMR antenna itself (distant target) is about 0.075, considerably larger than either that for the standard-gain horn (0.042) or that for the NOAA antenna at 54 GHz (0.031). Also, $|\Delta\Gamma|$ is considerably larger ($\sim$0.12 maximum) for the AIMR antenna–target combination, which will in turn lead to larger errors from its neglect. For all three antennas, a large target consisting of foam absorber has very little effect on the antenna reflection coefficient ($\Delta|\Gamma| \sim 0.001$).

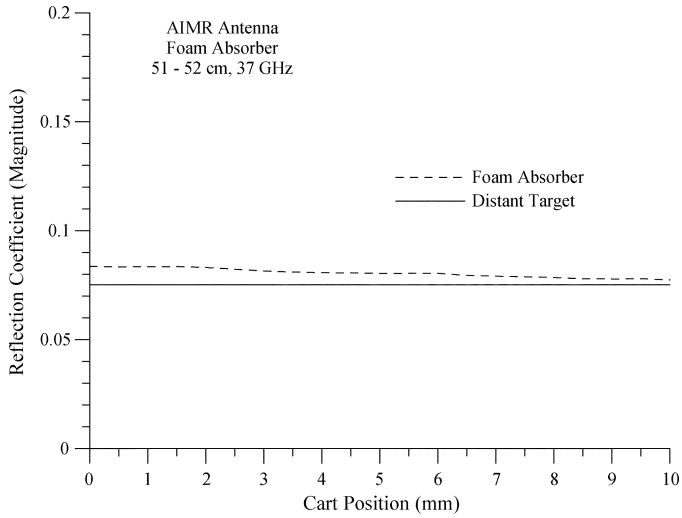

Fig. 9. Reflection coefficient of AIMR antenna viewing foam absorber.

C. Measurement of Noise Parameters

In order to estimate the error using (6), we also need to measure or estimate the noise parameters X_1 and X_{12} of the radiometer. They can be measured using a method similar to that suggested by Meys [12]. The method as applied here is outlined in Appendix B. To obtain realistic values for our estimates, we measured the noise parameters of the AIMR radiometer at 37 GHz, with the results that $X_1 \approx 223$ K and $|X_{12}| \approx 37.6$ K. The radiometer is designed with the IF mixers mounted directly on the four feed horn outputs, and consequently its noise parameters are set by the IF mixers.

Another convenient case to consider is a total-power radiometer with an isolator on the input. In that case, X_1 and X_{12} can be calculated; they are given by

$$X_1 \approx T_I \quad X_{12} \approx -T_I S_{11}^I \tag{7}$$

where I refers to the isolator, and we have assumed $|S_{11}^I|$, $|S_{22}^I|$, and $|S_{12}^I|$ are all small. Note that in this case $\Gamma_r \approx S_{11}^I$, and (6) leads to $\Delta_2 + \Delta_3 = 0$, so that the only remaining error is δ_1, which is due to the different mismatch factors. Representative numerical values are given in Section IV.

IV. Numerical Estimates

We can now estimate the magnitude of the error introduced by using the simple form of the radiometer equation, (3). From (4) and (6), the total error is given approximately by

$$\Delta_{\rm tot} \approx 2T_{x,0}\,{\rm Re}\,[(\Gamma_r - \Gamma_\infty)\Delta\Gamma] + 2X_1\,{\rm Re}(\Gamma_\infty \Delta\Gamma) + 2\,{\rm Re}(X_{12}\Delta\Gamma) \tag{8}$$

where $T_{x,0} = (T_x - T_a)_0 + T_a$. The value of Γ_r will obviously vary from one radiometer to another, but it will typically be small. If we set $\Gamma_r = 0$, it will have little effect on the numerical results and no effect on the qualitative conclusions. We, therefore, do so and refer to the resulting error and uncertainty as $\Delta^{(0)}$ and $u^{(0)}$. With $\Gamma_r = 0$, the total error takes the form

$$\Delta_{\rm tot}^{(0)} \approx 2(X_1 - T_{x,0}){\rm Re}(\Gamma_\infty \Delta\Gamma) + 2\,{\rm Re}(X_{12}\Delta\Gamma). \tag{9}$$

In evaluating the error and uncertainty for an actual radiometer, one would proceed as below but use the actual value of $(\Gamma_r - \Gamma_\infty)$ rather than Γ_∞ in the first term of (8) and (9).

We work in terms of the standard uncertainties u [13], [14]. These are estimates of the root mean square (RMS) values of the errors, where the mean is taken over reasonably probable measurement possibilities, which in this case means over reasonable values of the unknown parameters. Thus

$$u_{\rm tot}^{(0)} = \sqrt{\left\langle \left(\Delta_{\rm tot}^{(0)}\right)^2 \right\rangle} \tag{10}$$

where the brackets indicate an average over Γ_∞ and $\Delta\Gamma$, which we can evaluate from our measurement results for the configurations we considered. Substituting (9) into (10), we have

$$u_{\rm tot}^{(0)} = 2\left\{(X_1 - T_{x,0})^2 \left\langle \left({\rm Re}(\Gamma_\infty \Delta\Gamma)\right)^2 \right\rangle + \frac{1}{2}|X_{12}|^2 \left\langle |\Delta\Gamma|^2 \right\rangle \right\}^{\frac{1}{2}} \tag{11}$$

where we have averaged over the (unknown) phase between X_{12} and $\Delta\Gamma$, which introduces the factor of 1/2 in the second term. The remaining averages are over the distance between antenna and calibration target. They can be evaluated from our measured results.

We will treat two specific cases as a demonstration and to obtain representative results. Other cases and general features will be discussed in Section V. The first case is that of the AIMR antenna with the AIMR target (cover on) at the approximate operating distance in the radiometer, 34–35 cm. From our measurements, $X_1 = 223$ K, $|X_{12}| = 37.6$ K, $\langle({\rm Re}(\Gamma_\infty \Delta\Gamma))^2\rangle = 3.25 \times 10^{-5}$, and $\langle|\Delta\Gamma|^2\rangle = 0.009\,57 = |\Delta\Gamma|^2_{\rm RMS}$. Consequently, for values of $T_{x,0}$ in the range of 200–300 K

$$u_{\rm tot}^{(0)} \approx \sqrt{2}|X_{12}||\Delta\Gamma|_{\rm RMS} \approx 5.2 \text{ K}. \tag{12}$$

This is somewhat larger than would be expected from the checks comparing different calibration methods for this instrument [15]. Those tests indicated that the different methods yielded results that agreed to within about 2 K. There are at least three possible explanations for this apparent discrepancy. One is that the measurement of the AIMR noise parameters took much longer than the time over which the instrument is designed to be stable. Consequently, some drift would have occurred during the measurement, and the resulting value for $|X_{12}|$ may be an overestimate. The second possible explanation is that only the feed horn (without the reflector) of the AIMR radiometer was used in these tests, and the effect on the reflection coefficient of the full antenna may be less. Furthermore, the feed horn used was a spare, which was not necessarily identical to the feed horn in the actual radiometer. Finally, it should be borne in mind that the result for the standard uncertainty in (11) is an RMS value, with the average taken over a range of antenna-to-target distances, whereas the actual AIMR instrument corresponds to just one of those distances, which could well be a relatively fortunate one. In particular, the transition from (9) to (11) entailed an average of $[{\rm Re}(X_{12}\Delta\Gamma)]^2$ over the relative phase between X_{12} and $\Delta\Gamma$. If X_{12} and $\Delta\Gamma$ happen to be out of phase for AIMR, this dominant contribution to the error vanishes, and the remaining error is less than 1 K. (The distinction between "error" and "uncertainty" is important here—and elsewhere. The error is the difference between the value obtained and the true value. The uncertainty represents an RMS average expected value of the error).

If the radiometer had an isolator on the front end, then one would have $X_1 \approx T_a$, $X_{12} \approx -T_a S_{11}^I$, and the uncertainty can be substantially reduced provided $|S_{11}|$ of the isolator is small. If $|S_{11}| = 0.025$, $u_{\rm tot}^{(0)} \approx 1$ K for $|T_{x,0} - T_a|$ less than about 50 K.

The second case we consider is the NOAA antenna with the NASA target at 54 GHz. For this combination of antenna and target, $\langle({\rm Re}(\Gamma_\infty \Delta\Gamma))^2\rangle = 2.2 \times 10^{-9}$ and $|\Delta\Gamma|^2_{\rm RMS} = \langle|\Delta\Gamma|^2\rangle = 5.4 \times 10^{-6}$. The first term in (10) is, therefore, almost always negligible, and $u_{\rm tot}^{(0)} \approx 0.0033|X_{12}|$. The value of $|X_{12}|$ depends on the specific radiometer. Since $|X_{12}|$ could be of the order of 100 K or more, particularly at high frequencies, $u_{\rm tot}^{(0)}$ may well be several tenths of a kelvin. This is likely to be significant for many radiometers that are to be deployed in the next decade. If the radiometer has a front end isolator, $u_{\rm tot}^{(0)} \approx 0.95$ K $\times |S_{11}^I|$, and the uncertainty can be brought under 0.1 K for this combination of antenna and target.

V. Conclusion

We have considered the error arising from the difference in antenna reflection coefficient when viewing a distant scene and a nearby calibration target and using the common, simple form for the radiometer equation of a total power radiometer, (3). An expression was derived for the approximate error, and measurements were performed that enabled us to estimate the resulting standard uncertainty for some representative cases. For radiometers without front-end isolators, the uncertainty can be as large as several kelvins, depending on the particular antenna, target, and receiver. Even in relatively good cases the uncertainty can be a few tenths of a kelvin. Use of a well-matched isolator reduces the error significantly. The magnitudes of the antenna and receiver reflection coefficients and the target reflectivity are critical factors in determining the size of the error. For an unisolated radiometer, the receiver noise parameters are also important. Because of the variation of the effect with the distance between antenna and target, the situation in an actual case could be significantly better or worse than our estimates, which were RMS results for a range of distances and relative phases.

Our results suggest that for radiometers employing a calibration target close to the antenna, the effects of $\Delta\Gamma \neq 0$ need to be considered if uncertainties are to be of the order of a few kelvins or less. In that case, $\Delta\Gamma$ and Γ_∞ should be measured; Γ_r, X_1, and X_{12} should be measured or estimated; and the uncertainties should be estimated. In fact, if everything is measured, one can use the full radiometer equation, (2) or an equivalent form, and not worry about introducing errors by neglecting δ_1, Δ_2, and Δ_3. Our treatment assumed two nearby calibration targets and a distant scene. We expect an analogous effect when one of the calibration targets is nearby and the other is distant, such as cold space.

APPENDIX A

This appendix fills in a few of the steps leading from (5) to (6). We first assume that the effect is small, and so we keep only the lowest nonvanishing order in $\Delta\Gamma \equiv \Gamma_c - \Gamma_\infty$. If we first consider δ_1, and use $\Gamma_c = \Delta\Gamma + \Gamma_\infty$ to eliminate Γ_c, we can write

$$\begin{aligned}\delta_1+1 = \frac{M_c}{M_x} &= \frac{\left(1-|\Gamma_\infty+\Delta\Gamma|^2\right)|1-\Gamma_\infty\Gamma_r|^2}{\left(1-|\Gamma_\infty|^2\right)|1-\Gamma_\infty\Gamma_r-\Gamma_r\Delta\Gamma|^2} \\ &\approx \frac{\left[1-|\Gamma_\infty|^2-2\,\mathrm{Re}(\Gamma_\infty\Delta\Gamma)\right]|1-\Gamma_\infty\Gamma_r|^2}{(1-|\Gamma_\infty|^2)\{|1-\Gamma_\infty\Gamma_r|^2-2\,\mathrm{Re}\left[\Gamma_r\Delta\Gamma(1-\Gamma_\infty\Gamma_r)\right]\}}\end{aligned} \tag{A.1}$$

where terms of order $|\Delta\Gamma|^2$ have been neglected. To facilitate approximations, we rewrite this as

$$\frac{M_c}{M_h} \approx \left[1-\frac{2\,\mathrm{Re}(\Gamma_\infty\Delta\Gamma)}{(1-|\Gamma_\infty|^2)}\right]\left\{1-\frac{2\,\mathrm{Re}\left[\Gamma_r\Delta\Gamma(1-\Gamma_\infty\Gamma_r)\right]}{|1-\Gamma_\infty\Gamma_r|^2}\right\}^{-1}. \tag{A.2}$$

We then also assume that each of the reflection coefficients Γ_c, Γ_∞, and Γ_r is small, make repeated use of the expansion $(1-x)^{-1} \approx 1+x+\ldots$, and save only terms to the second order in the reflection coefficients. We can then write

$$\begin{aligned}\frac{M_c}{M_x} &\approx \left[1-\frac{2\,\mathrm{Re}(\Gamma_\infty\Delta\Gamma)}{(1-|\Gamma_\infty|^2)}\right]\left\{1+\frac{2\,\mathrm{Re}\left[\Gamma_r\Delta\Gamma(1-\Gamma_\infty\Gamma_r)\right]}{|1-\Gamma_\infty\Gamma_r|^2}\right\} \\ &\approx 1-\frac{2\,\mathrm{Re}(\Gamma_\infty\Delta\Gamma)}{(1-|\Gamma_\infty|^2)}+\frac{2\,\mathrm{Re}\left[\Gamma_r\Delta\Gamma(1-\Gamma_\infty\Gamma_r)\right]}{|1-\Gamma_\infty\Gamma_r|^2} \\ &\approx 1-2\,\mathrm{Re}(\Gamma_\infty\Delta\Gamma)+2\,\mathrm{Re}[\Gamma_r\Delta\Gamma]\end{aligned} \tag{A.3}$$

and therefore

$$\delta_1 \approx 2\,\mathrm{Re}\left[(\Gamma_r-\Gamma_\infty)\Delta\Gamma\right]. \tag{A.4}$$

Equation (A.4) includes only the lowest order terms in $\Delta\Gamma$ and in the Γ's. This expression depends on the relative phase of $(\Gamma_r-\Gamma_\infty)$ and $\Delta\Gamma$, and it can be very small or even vanish, depending on that phase. In such cases, the higher order terms become important. To reassure ourselves that this approximation is adequate for our purposes, we performed Monte Carlo computations comparing the exact expression, (5) and (A.1), with the approximation of (A.4), for sets of values of the Γ's encountered in our measurements. The computations indicated that there are significant differences between the exact and approximate forms in some cases, especially for small values of δ_1, as expected. For purposes of estimating uncertainties, however, where we average over the unknown phases, the difference between the exact and approximate values was only 3.5×10^{-4} in the worst case (AIMR horn with AIMR target). This is negligible in the uncertainty estimate, and consequently, we are safe in using (A.4) in our uncertainty estimates.

To simplify the equation for Δ_2, we use (A.2) for M_c/M_x as well as the equation that relates delivered spectral power to noise temperature, $p_h - p_c = M_c k(T_h - T_c)$. The result is

$$\Delta_2 \approx 2T_c\mathrm{Re}\left[(\Gamma_r-\Gamma_\infty)\Delta\Gamma\right]. \tag{A.5}$$

For Δ_3, we need to relate $(p_{e,x}-p_{e,c})$ to the noise parameters of the radiometer's receiver. The set of noise parameters that we use [9] are elements of the noise correlation matrix in the wave formulation [10], referred to the input port and converted to temperatures. To be more specific, let c_1 and c_2 be the amplitudes of the noise waves emanating from the input (1) and output (2) ports of an amplifier due to the intrinsic noise of the amplifier itself. Elements of the noise correlation matrix $\boldsymbol{N}$ are defined by $N_{ij} \equiv \overline{c_i c_j^*}$, where the bar indicates a time average. The X parameters we use are defined by $kX_1 = \overline{|c_1|^2}$, $kX_{12} = \overline{c_1 c_2^*}/S_{21}^*$, $kX_2 = \overline{|c_2|^2}$. The X's have dimensions of temperature, and because c_2 is scaled by $1/S_{21}$, they represent effective noise temperatures referred to the input plane (1) of the amplifier or receiver. In the present case, plane 2 is chosen inside the radiometer at some point after the component that sets the radiometer's noise figure. Thus, for example, if the radiometer has an amplifier in the input chain, plane two would be chosen after the amplifier. The noise temperature at plane 2 can then be related to the input noise temperature (plane 1) by [9]

$$\begin{aligned}T_2 = G_{21}\Bigg\{&T_1+\frac{|\Gamma_1|^2}{(1-|\Gamma_1|^2)}X_1+\frac{|1-\Gamma_1S_{11}|^2}{(1-|\Gamma_1|^2)}X_2 \\ &+\frac{2}{(1-|\Gamma_1|^2)}\mathrm{Re}\left[(1-\Gamma_1S_{11})^*\Gamma_1X_{12}\right]\Bigg\}\end{aligned} \tag{A.6}$$

where S_{ij} is the ij element of the scattering matrix between planes 1 and 2, Γ_1 is the reflection coefficient of the termination attached to plane 1 (the antenna in our case), and G_{21} is the available gain, given by

$$G_{21} = \frac{|S_{21}|^2\left(1-|\Gamma_1|^2\right)}{|1-\Gamma_1S_{11}|^2\left(1-|\Gamma_2|^2\right)} \tag{A.7}$$

where Γ_2 is the reflection coefficient at plane 2, looking toward the antenna. Since the output noise temperature is related to the effective input noise temperature T_e by $T_2 = G_{21}(T_1+T_e)$, (A.5) allows us to identify

$$\begin{aligned}T_e = \Bigg\{&\frac{|\Gamma_1|^2}{(1-|\Gamma_1|^2)}X_1+\frac{|1-\Gamma_1S_{11}|^2}{(1-|\Gamma_1|^2)}X_2 \\ &+\frac{2}{(1-|\Gamma_1|^2)}\mathrm{Re}\left[(1-\Gamma_1S_{11})^*\Gamma_1X_{12}\right]\Bigg\}.\end{aligned} \tag{A.8}$$

The p_e's of (5) in Section II are related to T_e through the mismatch factor at plane 1, $p_e = kM_1T_e$, enabling us to write

$$\begin{aligned}p_{e,x}-p_{e,c} &= k\left(1-|\Gamma_r|^2\right)\left\{\left(\frac{|\Gamma_\infty|^2}{|1-\Gamma_\infty\Gamma_r|^2}-\frac{|\Gamma_c|^2}{|1-\Gamma_c\Gamma_r|^2}\right)X_1\right. \\ &\quad\left.+2\mathrm{Re}\left[\left(\frac{\Gamma_\infty}{(1-\Gamma_\infty\Gamma_r)}-\frac{\Gamma_c}{(1-\Gamma_c\Gamma_r)}\right)X_{12}\right]\right\} \\ &\approx k\left[\left(|\Gamma_\infty|^2-|\Gamma_c|^2\right)X_1-2\,\mathrm{Re}(\Delta\Gamma X_{21})\right]\end{aligned} \tag{A.9}$$

where we have applied approximations similar to those used for δ_1 and Δ_2. If we then use (A.2) for M_c/M_x and $(T_h-T_c)/(p_h-p_c) = 1/(M_ck)$, Δ_3 can be written as

$$\begin{aligned}\Delta_3 &= -\frac{M_c}{M_x}\frac{(p_{e,x}-p_{e,c})}{(p_h-p_c)}(T_h-T_c) \\ &\approx 2X_1\mathrm{Re}\left(\Gamma_\infty\Delta\Gamma\right)+2\mathrm{Re}(\Delta\Gamma X_{12}).\end{aligned} \tag{10}$$

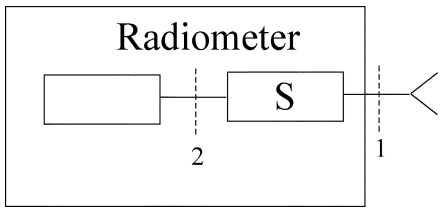

Fig. 10. Reference planes.

APPENDIX B

Although Meys [12] was interested in measuring the noise parameters of amplifiers, the method is directly applicable to radiometers. To apply the method to a remote sensing radiometer, we refer to Fig. 10. Plane 1 is defined as the plane at which the antenna is connected to the rest of the radiometer. Plane 2 is chosen at a point within the radiometer such that (A.5) holds, and such that Γ_2 is very nearly independent of Γ_1. This point need not be accessible; it need only exist. If the radiometer front end has a low-noise amplifier with good reverse isolation ($S_{12} \approx 0$), then this point could be at the amplifier output. If the radiometer has no front-end amplifier, plane 2 can be taken to be after the mixer. We assume that S_{11} is small, that the reflection coefficient looking to the left at plane 2 is small, and that the response R of the radiometer, be it power, voltage, or whatever, is related to the power delivered at plane 2 by

$$R = R_0 + A p_{2,\mathrm{del}}. \tag{B.1}$$

Moderate departures from our approximations on the reflection coefficients and S_{11} are not of concern. We are trying to estimate uncertainties, and such departures would contribute only to the uncertainty in the uncertainty.

The response of the radiometer for a given termination G at plane 1 can then be obtained from (B.1) and (A.5) by using $p_{2,\mathrm{del}} = M_2 p_{2,\mathrm{avail}} = k_B M_2 T_2$

$$R(G) = R_0 + A|S_{21}|^2 \left\lfloor \left(1 - |\Gamma_1|^2\right) T_1 + |\Gamma_1|^2 X_1 + X_2 + 2\mathrm{Re}(\Gamma_1 X_{12}) \right\rfloor \tag{B.2}$$

where M_2 is the mismatch factor at plane 2, and where we have absorbed inconsequential constants and factors into A. Meys' method consists of first determining the gain $(A|S_{21}|^2)$ and noise temperature for a reflectionless source ($T_{e0} = X_2$) by measuring a hot and a cold matched source, T_h and T_c with $\Gamma_1 \approx 0$. X_1 and X_{12} are then determined by a series of measurements with a sliding short on the input. The equations for the hot and cold matched loads become

$$\begin{aligned} R(h) &= R_0 + A|S_{21}|^2(T_h + X_2) \\ R(c) &= R_0 + A|S_{21}|^2(T_c + X_2) \end{aligned} \tag{B.3}$$

which lead to

$$\begin{aligned} A|S_{21}|^2 &= \frac{R_h - R_c}{T_h - T_c} \\ X_2 + \frac{R_0}{A|S_{21}|^2} &= \frac{T_h - Y T_c}{Y - 1}. \end{aligned} \tag{B.4}$$

Similarly, when the sliding short is attached to the radiometer input, the response is given by

$$R = R_0 + A|S_{21}|^2 \left(X_1 + X_2 + 2|X_{12}| \cos\phi\right) \tag{B.5}$$

where ϕ is the phase angle between X_{12} the reflection coefficient of the sliding short. A series of measurements for different positions of the sliding short, and consequently different values of $\cos\phi$, should yield a sinusoidal curve from which X_1 and $|X_{12}|$ can be determined. The equations for X_1 and $|X_{12}|$ are

$$\begin{aligned} X_1 &= \frac{\overline{R}}{A|S_{21}|^2} - \left(X_2 + \frac{R_0}{A|S_{21}|^2}\right) \\ |X_{12}| &= \frac{\Delta R}{4A|S_{21}|^2} \end{aligned} \tag{B.6}$$

where $\overline{R}$ is the average, and ΔR is the peak-to-peak difference of the sinusoidal pattern obtained for the response as one slides the short. The appearance in (B.4) of the term involving R_0 means that we cannot determine X_2 without some way to determine R_0. Fortunately, we do not need X_2 for our estimate of the uncertainties. The combination of X_2 and R_0 that appears in (B.6) is just what is determined in (B.4), and consequently we can determine X_1.

ACKNOWLEDGMENT

The authors are grateful to A. Gasiewski and V. Leuski (NOAA Environmental Technology Laboratory) for the loan of an antenna and for helpful discussions, to P. Racette and J. Piepmeier (NASA Goddard Space Flight Center) for the loan of a target and for helpful discussions, and to D. Camell (NIST) for assistance in using the NIST anechoic chamber. The authors are grateful to the Meteorological Service of Canada, Environment Canada (Atmospheric and Climate Science Directorate and Canadian Ice Service) for the use of the AIMR system.

REFERENCES

[1] J. P. Hollinger, J. L. Peirce, and G. A. Poe, "SSM/I instrument evaluation," *IEEE Trans. Geosci. Remote Sens.*, vol. 28, no. 5, pp. 781–790, Sep. 1990.

[2] T. Mo, "A study of the microwave sounding unit on the NOAA-12 satellite," *IEEE Trans. Geosci. Remote Sens.*, vol. 33, no. 5, pp. 1141–1152, Sep. 1995.

[3] C. S. Ruf, S. Keihm, and M. A. Janssen, "TOPEX/Poseidon Microwave Radiometer (TMR). I. Instrument description and antenna temperature calibration," *IEEE Trans. Geosci. Remote Sens.*, vol. 33, no. 1, pp. 125–137, Jan. 1995.

[4] D. Cimini, E. R. Westwater, Y. Han, and S. Keihm, "Accuracy of ground-based microwave radiometer and balloon-borne measurements during the WVIOP2000 field experiment," *IEEE Trans. Geosci. Remote Sens.*, vol. 41, no. 11, pp. 2605–2615, Nov. 2003.

[5] A. S. Milman and T. T. Wilheit, "Sea surface temperatures from the Scanning Multichannel Microwave Radiometer on Nimbus 7," *J. Geophys Res.*, vol. 90, no. 11, pp. 1631–1641, 1985.

[6] K. Foster and T. Hewison, "The absolute calibration of total power millimeter-wave airborne radiometers," in *Proce. IGARSS*, vol. 1, Jul. 6–10, 1998, pp. 384–386.

[7] A. J. Gasiewski and D. M. Jackson, "Electromagnetic scattering from microwave absorbers: Laboratory verification of the coupled wave theory," in *Proc. 1992 APS Int. Symp.*, Chicago, IL, pp. 412–415.

[8] D. M. Jackson, "Calibration of millimeter-wave radiometers with application to clear-air remote sensing of the atmosphere," Ph.D. thesis, Georgia Inst. Technol., Atlanta, 1999.

[9] J. Randa, "Noise-parameter uncertainties: A Monte Carlo simulation," *J. Res. NIST*, vol. 107, pp. 431–444, Sep./Oct. 2002.
[10] S. W. Wedge and D. B. Rutledge, "Wave techniques for noise modeling and measurement," *IEEE Trans. Microwave Theory Tech.*, vol. 40, no. 11, pp. 2004–2012, Nov. 1992.
[11] M. J. Collins, F. G. R. Warren, and J. L. Paul, "The Airborne Imaging Microwave Radiometer—Part I: Radiometric analysis," *IEEE Trans. Geosci. Remote Sens.*, vol. 34, no. 2, pp. 643–655, Mar. 1996.
[12] R. P. Meys, "A wave approach to the noise properties of linear microwave devices," *IEEE Trans. Microwave Theory Tech.*, vol. MTT-26, no. 1, pp. 34–37, Jan. 1978.
[13] ISO, "ISO guide to the expression of uncertainty in measurement," Int. Standards Org., Geneva, Switzerland, 1993.
[14] B. N. Taylor and C. E. Kuyatt, "Guidelines for evaluating and expressing the uncertainty of NIST measurement results," Nat. Inst. Standards Technol., Gaithersburg, MD, NIST Tech. Note 1297, 1994.
[15] J. Haggerty, A. Cox, and C. Walther, "Extending the calibration range for the Airborne Imaging Microwave Radiometer (AIMR) part II: Using the sky for low temperature calibration points," presented at the *1st Int. Microwave Radiometer Calibration Workshop*, College Park, MD, Oct. 30–31, 2000.

James Randa (M'89–SM'91) received the Ph.D. degree in physics from the University of Illinois, Urbana, in 1974.

He then held Postdoctoral and/or faculty positions at Texas A&M University, the University of Manchester, and the University of Colorado at Boulder. During this time, he did research on the phenomenology of elementary particles and on theories of fundamental interactions. Since 1983, he has been with the Electromagnetics Division, National Institute of Standards and Technology (NIST), Boulder, CO. From 1983 to 1994, he was in the Fields and Interference Metrology Group, working on various topics in EMI metrology. Since early 1994, he has been in the RF Electronics Group of NIST, where he heads the Thermal Noise Metrology Project.

David K. Walker (M'97) received the B.A. degree in physics and mathematics from Hastings College, Hastings, NE, in 1980, and the B.S. and M.S. degrees in electrical engineering from Washington University, St. Louis, MO, in 1982 and 1983, respectively. He spent eight years in industry working on microwave semiconductor device design and fabrication before joining the National Institute of Standards and Technology (NIST), Boulder, CO, in 1991 as part of the MMIC Project in the Microwave Metrology Group. His work at NIST has included semiconductor fabrication, network analyzer calibration, and on-wafer measurements. Current research interests include microwave thermal noise measurements and calibration of radiometers for remote sensing. He holds five patents related to microwave technology.

Amanda E. Cox (S'96–M'03) received the B.S. degree in electrical engineering, the M.S. degree in aerospace engineering sciences, and the Ph.D. degree in aerospace engineering, in 1983, 1996, and 2004, respectively, all from the University of Colorado, Boulder.

She is currently a Research Associate with the National Institute of Standards and Technology, Boulder, CO. She has worked previously as a Guest Researcher and Graduate Fellow with the National Center for Atmospheric Research, Boulder, CO, as a Senior Systems Engineer at Ball Aerospace Corp., Boulder, CO, and as a Project Engineer with both Teledyne MEC, Palo Alto, CA, and TIW Systems, Sunnyvale, CA. Her research interests include remote sensing, microwave radiometry, and GPS.

Robert L. Billinger received the Associates degree in electronics technology from Wichita Technical Institute, Wichita, KS, in 1979.

From 1979 to 1984, he was with PureCycle Corporation, where he became Manger of Mechanical and Electronic Production and Test. Since 1985, he has been with the Electromagnetics Division, RF Electronics Group, National Institute of Standards and Technology, Boulder, CO, where he is an Electronics Technician working in the area of thermal noise.